Wind loads on fixed-roof cylindrical tanks with very low aspect ratio

Yin Lin and Yang Zhao[*]

Spatial Structures Research Center, Zhejiang University, Hangzhou 310058, China

Abstract. Wind tunnel tests are conducted to investigate the wind loads on vertical fixed-roof cylindrical tanks with a very low aspect ratio of 0.275, which is a typical ratio for practical tanks with a volume of 100,000 m^3. Both the flat-roof tank and the dome-roof tank are investigated in present study. The first four moments of the measured wind pressure, including the mean and normalized deviation pressure, kurtosis and skewness of the pressure signal, are obtained to study the feature of the wind loads. It is shown that the wind loads are closely related to the behavior of flow around the structure. For either tank, the mean wind pressures on the cylinder are positive on the windward area and negative on the sides and the wake area, and the mean wind pressures on the whole roof are negative. The roof configurations have no considerable influence on the mean pressure distributions of cylindrical wall in general. Highly non-Gaussian feature is found in either tank. Conditional sampling technique, envelope method, and the proper orthogonal decomposition (POD) analysis are employed to investigate the characteristics of wind loads on the cylinder in more detail. It is shown that the patterns of wind pressure obtained from conditional sampling are similar to the mean pressure patterns.An instantaneous pressure coefficient can present a wide range from the maximum value to the minimum value. The quasi-steady assumption is not valid for structures considered in this paper according to the POD analysis.

Keywords: wind load; fixed-roof tank; wind tunnel test; non-Gaussian feature; conditional sampling; POD analysis

1. Introduction

Vertical cylindrical tanks are widely used for the storage of fluid or bulk in industrial plants (Myers 1997). They are typical thin-walled shell structures and are thus very susceptible to buckling under wind loads which is a major consideration in the design.

Destructions of cylindrical tanks during wind storm (sometimes even under moderate wind loads) have been occurred in many countries and regions over the past few decades (Sosa 2005, Godoy 2007, Godoy and Jaca 2010), resulting in serious consequences including economic losses and environmental problems. One of the main challenges for the designers is the scarcity of reliable wind loads on tanks. Therefore wind pressure distributions on tanks have been studied extensively in the past (e.g., Maher 1966, Purdy *et al*. 1967, Macdonald *et al*. 1988, Portela and

*Corresponding author, Professor, E-mail: ceyzhao@zju.edu.cn

[a] Ph. D. Student, E-mail: yinlin@zju.edu.cn

Godoy 2005). However, there has been hardly any study concerned with super large tanks which are usually with an aspect ratio (*H/D*, height-to-diameter ratio for the cylindrical part) smaller than 0.3. Chinese Codes [viii] recommend adopting the same wind pressure distributions as other cylindrical buildings, ignoring that most large steel tanks are usually designed with smaller aspect ratio compared to other cylindrical structures. For typical tanks with a volume larger than 100, 000m^3, the information about wind loads is extremely limited. Other design standards including Eurocode and ASCE are also far behind on these aspects and much additional research is needed to upgrade them (Rotter 2009).

This paper investigates the wind loads on the tanks with a very low aspect ratio of 0.275, which is the most common dimension for tanks with a volume of 100,000 m^3. The study includes tanks with two roof types: flat roof and dome roof. The wind pressures on tanks with different types of roof were measured in the wind tunnel with scale rigid models. The first four moments of the measured wind pressure, including the mean and normalized deviation wind pressure, kurtosis and skewness of the pressure signal, are calculated and analyzed. A flow visualization simulation by numerical method is adopted to illustrate the wind field feature and its impact on the wind loads. The conditional sampling technique, envelope method, and the proper orthogonal decomposition (POD) analysis are employed to investigate the characteristics of wind loads on the cylinder in more detail.

2. Wind tunnel test

2.1 Experimental apparatus

Wind tunnel tests were carried out in a closed-loop wind tunnel at Zhejiang University, whose working section was 4 m(width) × 3 m(height) ×18 m(length).

A turbulent boundary layer flow was simulated by roughness elements on the tunnel floor to be appropriate to the sea-shore terrain where tanks are usually constructed. The power law exponent of the profile of mean wind velocity was 0.12. The wind velocity scale was set to 1/5. The mean wind velocity and the turbulence intensity at the top of cylinder part of model were 8.1 m/s and 15%, respectively as shown in Fig. 1(a). The wind velocity spectrum of the wind tunnel flow is shown in Fig. 1(b) and is compared with the Davenport spectrum and Karmal spectrum.And the corresponding Reynolds number based on D_m (cylinder diameter of model) and U_b (inflow velocity atthe top of cylinder) was 2.16×10^5.

2.2 Tank models

For practical tanks with a volume of 100,000 m^3, the common dimension of the cylinder is 80m in diameter and 22 m in height, therefore the aspect ratio of cylindrical part is 0.275. The study includes tanks with two roof types: flat roof and dome roof. Two different models used in the experiments had the same geometry on cylinder of 0.11 m in height and 0.4m in diameter but different roof types, flat roof and dome roof, as shown in Fig. 2. The dome roof radius was 1.0*D* in present study. The geometric scale was 1/200. The models were fabricated using fiber glass as well as engineering plastics. 144 pressure taps were installed at 4 levels in the cylindrical part and 109 pressure taps were installed at 5 levels in the roof (Fig. 2). The pressure taps were installed at intervals of 10°on the external surface of cylinder at each level along circumference and intervals

of 15° (intervals of 30°at the innermost layer and an additional tap at the apex) on the roof. The test models placed in the wind tunnel are shown in Fig. 3.

(a)   (b)
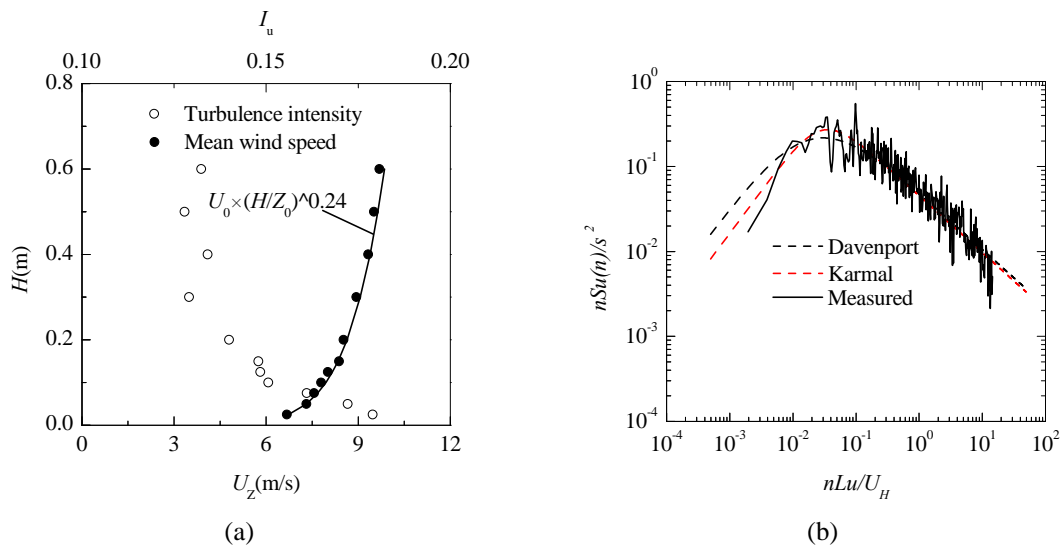
Fig. 1 Wind profile and spectrum in wind tunnel: (a) mean wind velocity and turbulence intensity and (b) velocity spectrum in height of 0.1 m
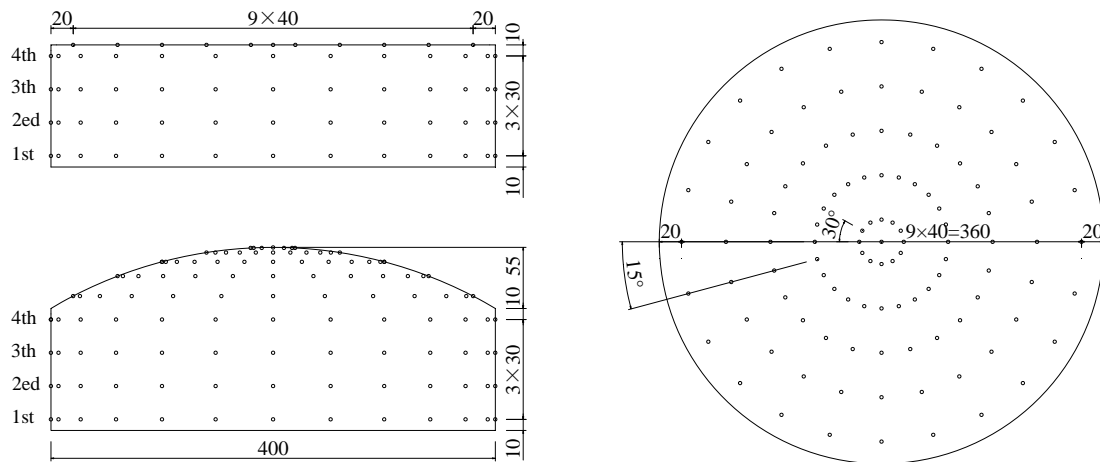
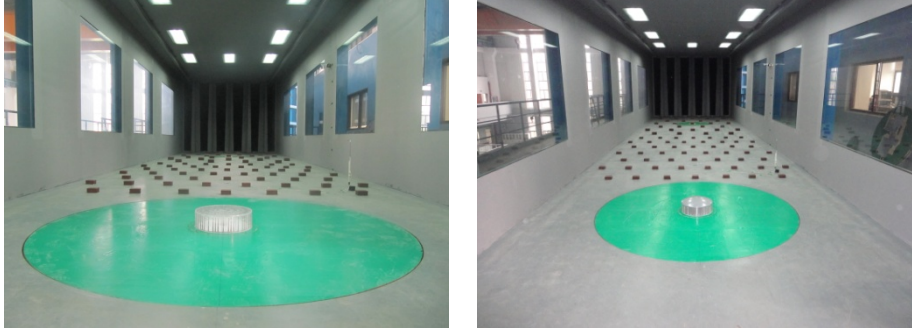

Fig. 2 Configuration of wind tunnel models (unit: mm)

Fig. 3 Test models installed in wind tunnel

2.3 Data acquisition

The wind pressures at all taps were sampled using a multi-channel dynamic pressure measurement system. The sampling frequency was 312.5 Hz, and 4,800 samples were collected continuously.

According to the general practice, the non-dimensional pressure coefficient $C_{pi}(\theta,z,t)$ is used to describe the instantaneous pressure $p_i(\theta,z,t)$ measured from the wind tunnel test, calculated as

$$C_{pi}(\theta,z,t) = \frac{p_i(\theta,z,t) - p_\infty}{\rho v_\infty^2 / 2} \tag{1}$$

where $p_i(\theta,z,t)$ is the total pressure of the tap, p_∞, ρ, v_∞ is the static pressure, density and wind velocity of the incoming flow at the cylinder top of the model, respectively.

The first two moments, time-mean and deviation pressure coefficient, denoted by C_{pi}^m and C_{pi}^r, respectively, are defined as following

$$C_{pi}^m = \frac{1}{N}\sum_{j=1}^{N} C_{pi} \tag{2}$$

$$C_{pi}^r = \sqrt{\sum_{j=1}^{N} \frac{C_{pi}^j - C_{pi}^m}{N-1}} \tag{3}$$

where N is number of samples.

The other two moments of the pressure distributions, skewness S and kurtosis K, are calculated as following

$$S_{pi} = \frac{(C_{pi} - C_{pi}^m)^3}{(N-1)C_{pi}^{r\,3}} \tag{4}$$

$$K_{pi} = \frac{(C_{pi} - C_{pi}^m)^4}{(N-1)C_{pi}^{r\ 4}} \quad (5)$$

S and *K* are usually used to describe the non-Gaussian feature. For Gaussian variable, $S_{pi} = 0; K_{pi} = 3$.

3. Air flow analysis

Smoke flow visualization tests were carried out in some previous studies as an aid in the explanation of the air flow behaviour over and around the models (Holroyd 1983, Sabransky 1987). In present study, numerical simulation is conducted to describe the complex air flow when passing around the tanks. It may help us to more easily understand the pattern of wind pressure distribution to be discussed later.

The software package Fluent is employed to carry out the simulation. Fig. 4(a) shows the computational domain for the simulation of flow around a flat-roof tank. The computational domain is chosen to be approximately $23H \times 14H \times 7H$. The non-slip wall boundary conditions are defined at the tank model surfaces and the terrain. The velocity inlet condition is specified at upstream boundary while the pressure outlet condition is specified at the downstream boundary. The symmetry boundary conditions are used at the top and lateral surfaces of the computational domain. The upstream and downstream boundaries are approximately located at $7H$ and $16H$, respectively, measured from the centre of model. Both the left and right boundaries are approximately located at $7H$ measured from the centre of model. Fig. 4(b) shows the grid distribution of the whole flow domain. The tetrahedron element is used to discretize the main body of the flow domain and the wedge element is used to discretize the flow domain near the tank model surfaces as a transition. The grid size grows from the model surfaces to the computational domain boundaries by using the size function.
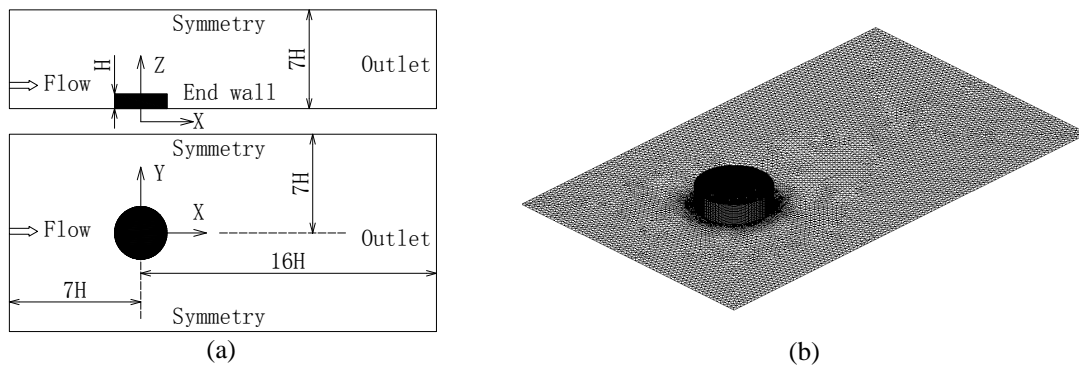

Fig. 4 Computational domain and grid distribution for simulation (a) computational domain and (b) grid distribution

The wind speed vector graphs of the vertical cut plane at windward meridian are given in Fig. 5(a) for flat-roof tank and Fig. 5(b) for dome-roof tank, respectively. The length and the arrows represent the magnitude and the direction of the wind flow. In either case, the wind velocity still presents a power law in the area near the tank. As the flow is very close to the structure, the wind velocity decreases rapidly and no longer keeps a power law. The wind velocity is a bit larger in the waist than in the upper and lower parts, with a vortex at the bottom. The maximum wind velocity is found at the height of approximate $Z=2/3H$ (H is the height of cylinder) which is the height of the 3^{th}level taps on the test models. Although the flow approaching tanks seems quite similar between the flat-roof tank and dome-roof tank, the air steams crossing the roof show significant difference. A vortex is found in the front of the flat roof and the wind velocity varies relatively rapidly there. In the rearward the flow is stable and wind velocity changes slightly. The wind flow keeps steady relatively when passing the dome roof. The wind velocity increases from the leading edge, reaches a peak value in the apex and then decreases to the leeward. The wind field exhibits a symmetry feature on the dome roof in some degrees.

The wind speed vector graphs of horizontal cut plane at height of $2/3H$ are given in Fig. 6. It can be seen that the incoming flow separate and then reattach on the side of cylinder for both models. The flow separation on the tanks with a flat roof is stronger than that on the dome one and the flow in wake region also presents somewhat difference. It will be seen later that the main difference of mean wind pressure distribution between the two models can be found on the side and the wake region of the cylinder. For both models, the vortex in wake region is not strong based on the simulation. This is probably due to the limitations of the turbulence model.
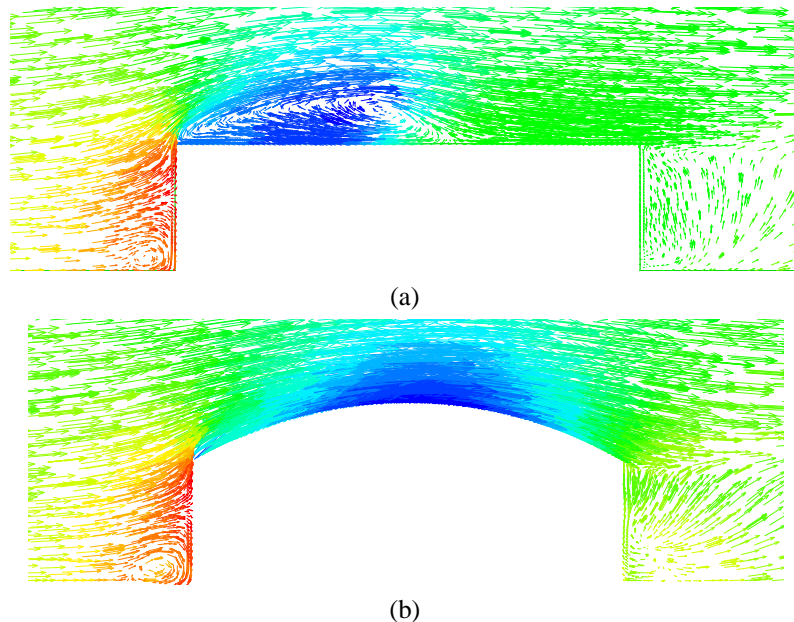

(a)

(b)

Fig. 5 Wind speed vector of the vertical cut plane (a) flat-roof tank and (b) dome-roof tank
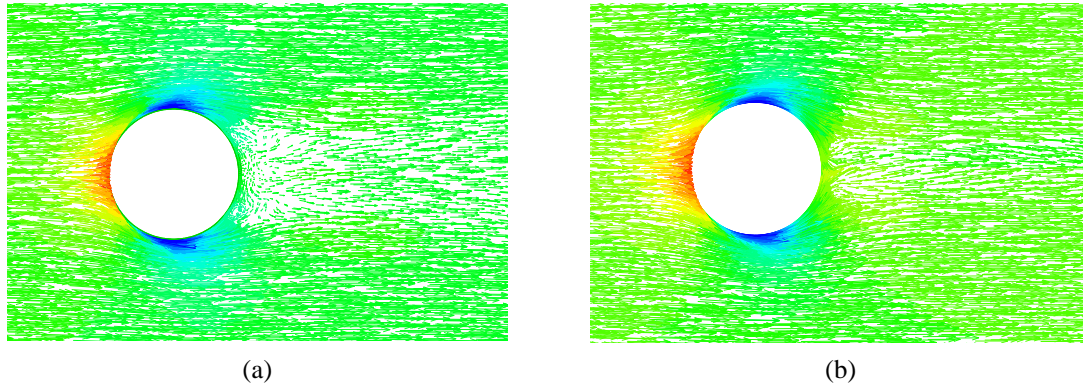
(a)　　　　　　　　　　　　　　　　　　(b)

Fig. 6 Wind speed vector of horizontal cut plane (a) flat-roof tank and (b) dome-roof tank

4. Results and discussion

4.1 Wind pressure on the cylinder

The first four moments of wind pressure signal denoted by contour plots are shown in Fig. 7 for the cylinder of the flat-roof tank. Results from both sides of the windward meridian were averaged according to the symmetry.The horizontal axis represents the attack angle measured from the windward medium.

Fig. 7(a) shows the mean pressure distribution on the cylinder of the flat-roof tank. The maximum positive mean pressures are found on the windward meridian while the peak suctions occur at around $\theta= 90°$, which agree well with the wind velocity vector field discussed above (Section 3).The coefficient of stagnation point is about 0.803,which means that the incident wind velocity there is about 11% lower than the reference full-stream value and reveals the behaviour of how the air flow distorted by the tank in order to bypass the tank according to Holroyd (1983).The mean pressure varies from positive values on the front to negative values on the side and rear, passing through zero around $\theta=42.5°$ which indicates that flow are very weak there and transit from stagnation to separation state. Complete flow separation occurs at about 140°, after which the wind pressures remain relatively constant.

Fig. 7(b) shows the normalized deviation distribution on the cylinder of the flat-roof tank.It can be seen that the turbulence levels of the incident flow have been amplified by the tank wall, which is between 1~3 times larger on most of the cylinder except the rear region than that of the incident flow. In Holroyd's study (1983), the turbulence levels of the incoming flow were about 1/3 of present study, and the effects of flow distortion and turbulence amplification could reach up to 5 times, much higher than present case. This means that for the incoming flow with intense turbulence, the structure influence on the distortion would be relatively limited.

The third and fourth moments of the pressure distributions are shown on Figs. 7(c) and 7(d). The skewness varies from about 0.5 on the windward meridian to -0.3 in the wake region. And the Gaussian value is observed around $\theta= 50°$ while a minimum value of about -1.5 is obtained near the rim at $\theta = 110°$. The kurtosisvalues area little bigger than 3 on most of the cylinder surface, except the region near the up rim between $\theta = 100°~140°$where the skewness also approaches the

most noticeable non-Gaussian feature. The maximum value of the kurtosis in this region is up to about 6. In a word, the wind pressures all over the cylinder are quite different from Gaussian variable which indicates that it is not feasible to evaluate the peak value of wind loads base on the probability of the normal distribution.

Wind pressures on structures can usually be considered as the result of superposition of a large number of different sizes of point vortices according to the point vortex models (Sun *et al.* 2007). When there is a weak correlation between taps, the pressures will come out to be more or less Gaussian characteristics according to the central limit theorem. However, if the organized vortexes appear when the airflow passes structure, the pressures will present highly non-Gaussian property. Therefore, the non-Gaussian feature of the wind pressures suggests that there is a strong correlation between the different series of pressures.
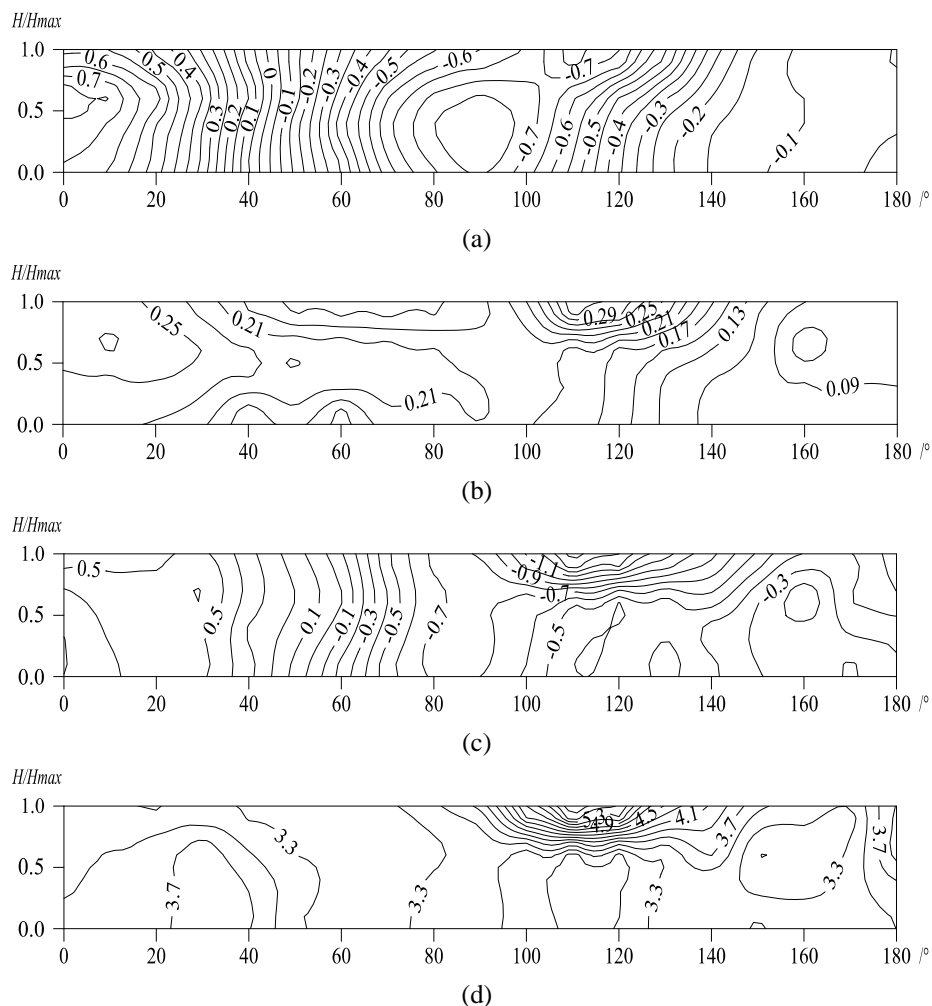

Fig. 7 First four moments of wind pressure coefficient on cylinder of flat-roof tank (a) mean (b) normalized deviation (c) skewness and (d) kurtosis
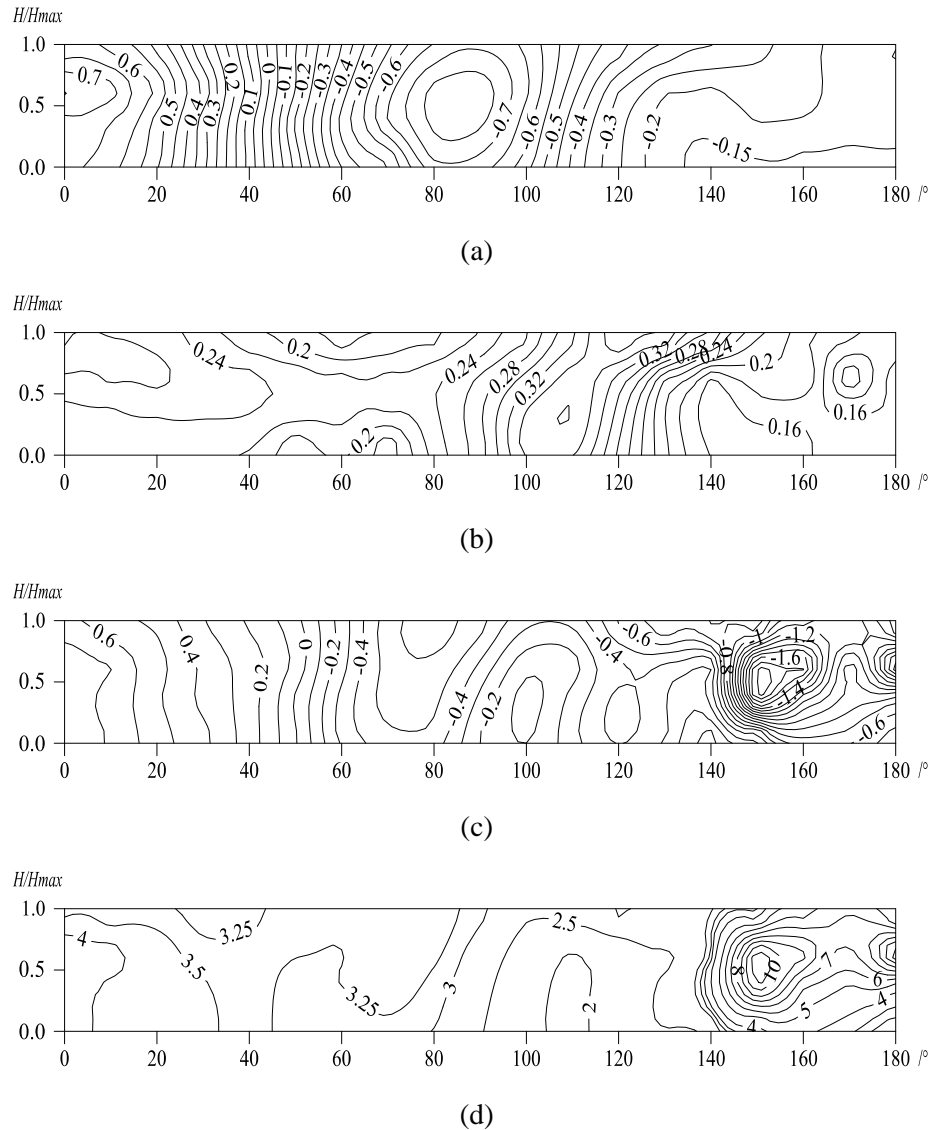
Fig. 8 First four moments of wind pressure coefficient on cylinder of dome-roof tank (a) mean (b) normalized deviation (c) skewness (d) kurtosis

The first four moments of wind pressure signal on the cylinder of the dome-roof tank are given in Fig. 8.

The mean pressure pattern on cylinder of the dome-roof tank (Fig. 8 (a)) is similar to that of the flat-roof tank with a same aspect ratio, although the values attached to them and some local trends

are slightly different. The maximum positive pressure on the windward meridian slightly decreases in comparison to that of the flat-roof tank. And the zero pressure obtained for dome-roof tank is in the angle of about 42.5°. This means that the dome-roof tank has an approximate same range of positive pressure outside the cylinder with the flat-roof tank. Suctions on the wake region slightly increase in comparison to that of the flat-roof tank.

Though the mean pressure pattern is similar to that of the flat-roof one, the deviation of pressures somehow present more different for the dome-roof tank (Fig. 8(b)). On the first half part of cylinder ($\theta = 0\sim90°$), the deviation values do not make a great deal of difference from those of the flat-roof tank. But for the second half part ($\theta = 90\sim180°$), the is obar is relatively compact and the deviation values are slightly larger than those of flat-roof tank which indicates that the fluctuations of wind flow on the side and wake regions are fiercer compared to those of the flat-roof tank.

Associated with the fluctuation of wind pressure, the skewness and kurtosis of pressure for dome-roof tank (Figs. 8(c) - 8(d)) also present a significant difference compared to those of the flat-roof tank. Theis obar is relatively compact which means that skewness and kurtosis gradient is larger than that of the flat-roof one in general. The values of both positive and negative skewness are larger than those of the flat-roof tank, and the skewness value is up to -1.9 on the rear for the dome-roof tank. Examine the kurtosis of the pressure signal of the dome-roof tank, it can be seen that the value on the first half part is larger than the Gaussian value, and the largest value is a little larger than that found on the flat-roof tank. The highly non-Gaussian taps are detected on the rear and the maximum value is up to 11. It is much larger than data obtained from the flat-roof model. On the region where flat-roof tank present a highly non-Gaussian feature the kurtosis of the dome-roof tank maintains a relatively lower level.
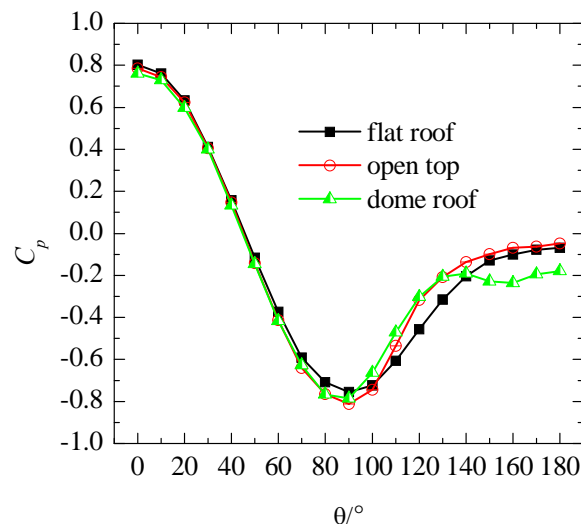

Fig. 9 Pressure on the external surface obtained from different model

Wind tunnel test on some silo models with a larger aspect ratio by Macdonald *et al.* (1988) investigated the effect of roof configuration including open top. However, the data used for open-top model was the net pressure (pressure difference between the external and internal pressure), while the pressure outside wall was not discussed alone. In present study, a tank model with open-top is used to measure the pressure distribution outside the wall for comparison with those with fixed roofs. Fig. 9 shows the pressure distributions on the external wall of cylinder for models with different roofs. It can be seen that the pattern is similar among the three models and only the pressures on the region of $\theta > 100°$ have slightly deviation. Thus, the roof configurations including the open-top have only little influence on pressure distributions on the external wall.

4.2 Wind pressure on the roof

Wind loads on roofs are vital not only for the design of a roof which is not self-supported but also for the overturning moments of the whole structure (Sabransky 1987).

The contour plots of pressure for the flat roof and the dome roof are given in Fig. 10. Although the mean pressure distribution pattern on cylinder is similar between the two models, the pressure distributions on the roof are much different, which agree well with the wind velocity vector field discussed above (Fig. 5). For the flat roof, the pressure is negative all over the whole roof, as is shown in Fig. 10(a). The highest negative mean pressure is found in the windward eaves where the suction coefficient is up to -1.2. Suction pressures decrease from the windward eaves to leeward eaves, exhibiting a quick descent on the front and relatively slow falling on the rear. For the dome roof, the pressure is also negative all over the whole roof, as is shown in Fig. 10(e). The highest negative mean pressure is not found in the windward eaves but around the apex of roof. And the peak suction value is about 0.70 which is 40% smaller than that on flat roof. Suctions increase from the windward leading edge to the apex of roof and then decrease to the trailing edge. The pattern seems symmetrical along the middle approximately.

The standard deviation pressure coefficients are given to understand the stability of the flow when passing over the roof. Fig. 10(b) shows the deviation distribution of the flat roof. Notice that the incoming flow turbulence identity is about 0.15 at the height of roof. The largest deviation pressure coefficient is found at the leading edge whose value is more than twice of the incoming flow, meaning that the flow is highly unstable there. As the flow goes ahead, the flow is back to the turbulence level of the incoming flow, even exhibiting a lower turbulence identity compared to the incoming flow at the leeward edge.

Figs. 10(c) and 10(d) show the skewness and kurtosis of pressure signals on the flat roof. The fierce non-Gaussian taps are observed at the both wings where the minimum skewness value is up to -1.3 and the maximum kurtosis value is up to 7.2.For the whole roof, the skewness values are negative with a smallest magnitude of around 0.2 at the leeward region.

Unlike the flat roof, the standard deviation pressure coefficients on the dome roof do not present remarkable change, as is shown in Fig. 10(f). The turbulence identity level is relatively close to the incoming flow although on some regions the value is a little larger or smaller than the incoming flow.

Although the flow is relatively stable, the non-Gaussian feature is found on most regions of the dome roof, as can be clearly observed from Figs. 10(g) and 10(h). The skewness values vary from 0.7 at the leading edge to -0.6 at the leeward region, with a Gaussian value at the middle of the first half part and a value of -0.4 at the middle of the latter part. The kurtosis value pattern is similar to the skewness to a certain extent. A Gaussian value is observed around the middle part.
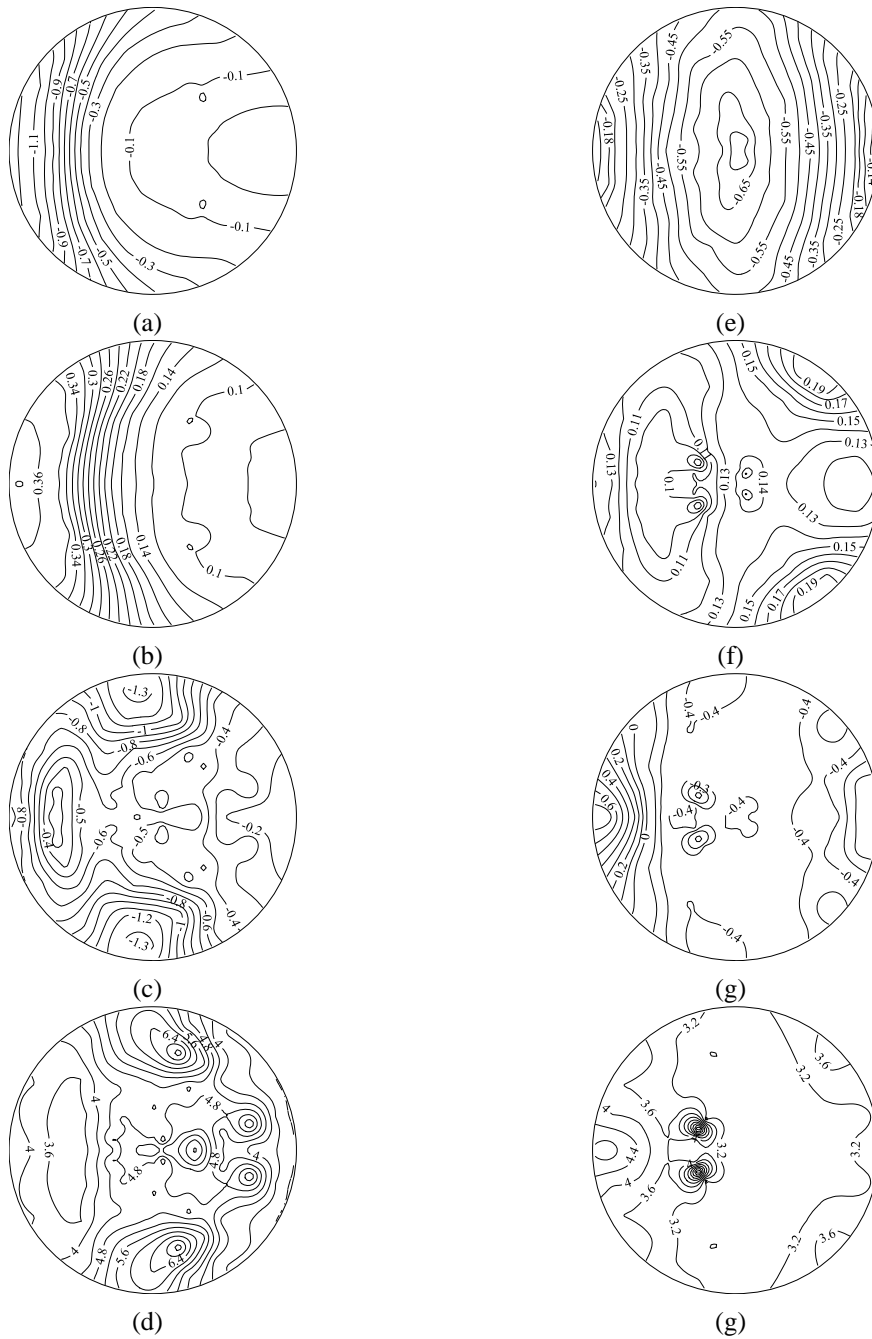
Fig. 10 First four moments of pressure signal on roofs (a)~(d) mean, deviation, skewness, kurtosis of the flat roof (e)~(h) mean, deviation, skewness, kurtosis of the dome roof

The kurtosis value at the windward eaves is 4.8, decrease at first and then increase rapidly at the regions near the apex, where the kurtosis is up to about 6.7. Unlike the first half part, the kurtosis value of the latter part of the roof is only a little larger than the Gaussian value.

4.3 Conditional sampling

As found in previous failures, the buckling of tanks usually occurs in the upper windward area of the cylindrical shell. Results from experiment and numerical simulation indicate that buckling behaviour of cylindrical shells seems dependent on the magnitude and extent of positive wind loads on the windward area (Choongmo 2010). A conditional sampling is carried out when the wind pressure at the tap in the windward meridian of 3th level (Z/H=0.64) presents the maximum positive value, because such a pressure distribution is very important from the viewpoint of structural stability of the shells (Uematsu 2008).The sample results are shown in Fig. 11 for the whole cylinder and Fig. 12 for the height of 0.64*H*. The patterns of pressure distribution by conditional sampling seem to be similar to those obtained by time-average. But a slight difference can be found when studying the detail. Take the coefficients at *Z*=0.64*H* for example (Fig. 12, both data have been normalized by the values at the stagnation point), the extents of positive pressure on the cylinder are somewhat narrower than those of mean pressure coefficients and the values are marginally bigger at the same positions. This situation was also observed on those with an open top by Uematsu (2008). However, the results by Uematsu are not completely coincident with present study. They found that the values in the leeward region are much smaller in magnitude than that of mean pressure coefficients. But in present study the magnitudes of most negative pressure are only slightly smaller than those of mean pressure coefficients for the flat-roof tank. When viewed as a whole, the distributions of conditional sampling are relatively steeper than those of mean pressure coefficients.
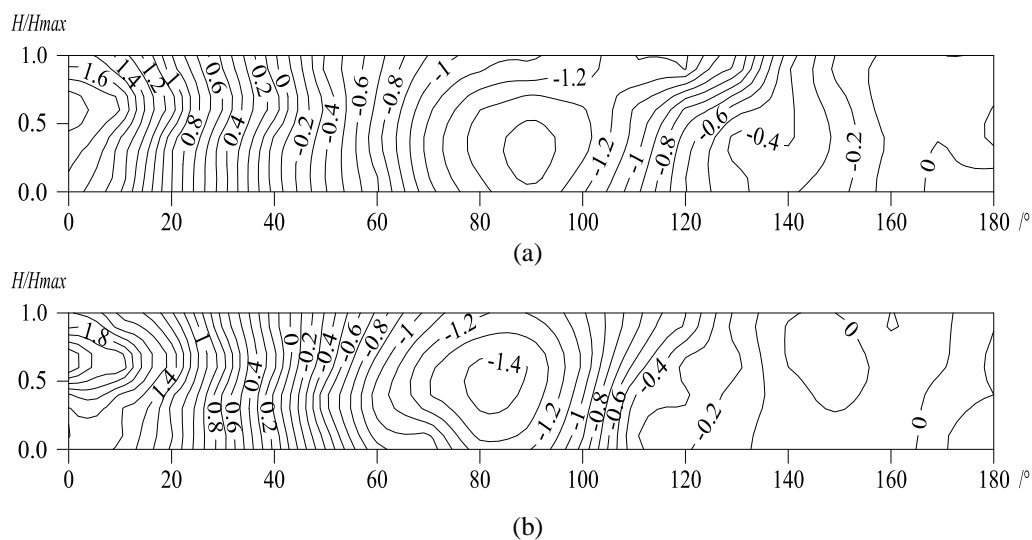

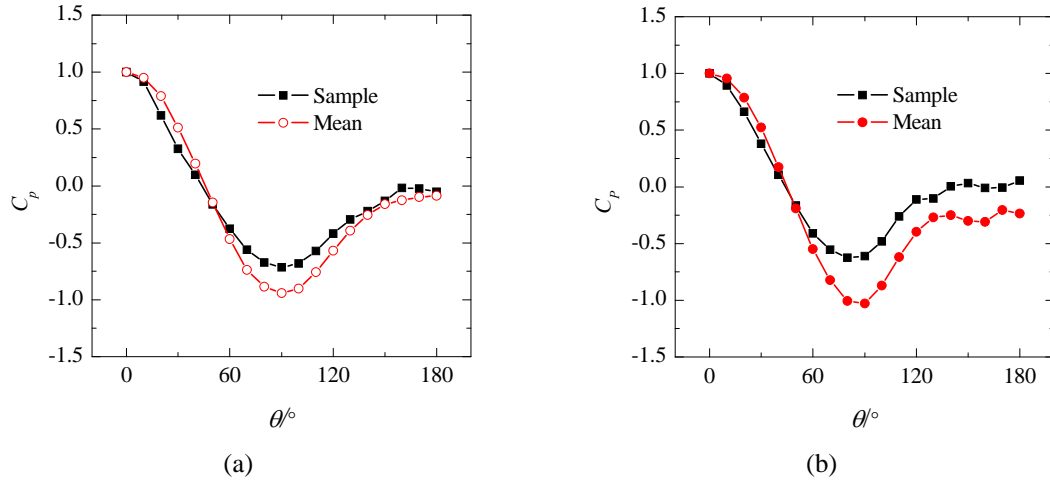Fig. 11 Pressure distribution by conditional sampling (a)flat-roof tank and (b) dome-roof tank

Fig. 12 Pressure distribution (Z=0.64H) by conditional sampling (a) flat-roof tank and (b) dome-roof tank
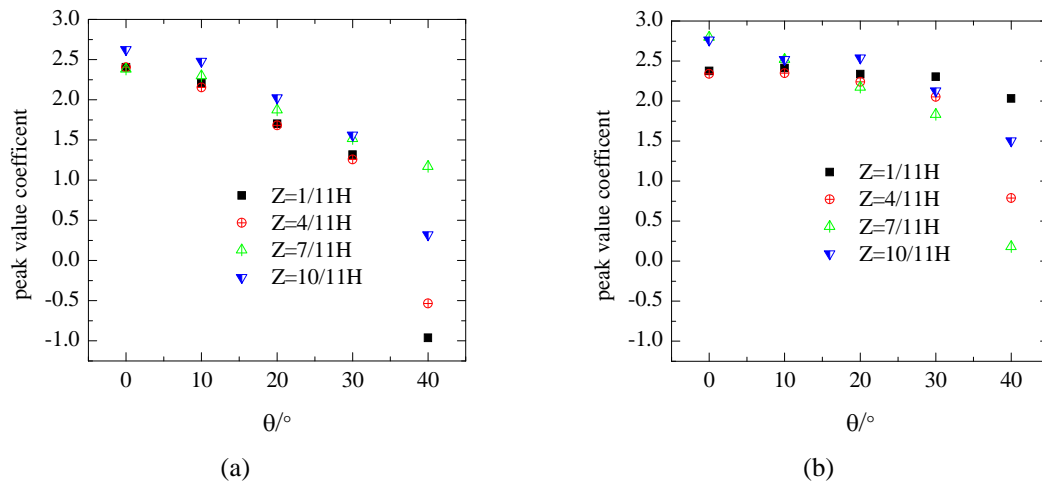

Fig. 13 Instantaneous peak value coefficient (a) flat-roof tank and (b) dome-roof tank

In structural aspect, designers are not only concerned with the time-mean wind loads but also the instantaneous peak values which can be expressed as a gust effect factor. As stated above, buckling of the cylindrical wall of tanks is mainly determined by the positive loads on the windward region. Thus, gust effect factor can be defined as the maximum instantaneous peak value coefficient based on the time-mean pressure in the positive pressure area in front of cylindrical wall. The instantaneous peak value coefficients for taps in the positive area are given in Fig. 13. The maximum coefficient is found at taps in the windward meridian of the 4th level (top level) for flat-roof tank and the 3th level for dome-roof tank.

4.4 Envelope and correlation

The envelope load is an other important load characteristic for designers. The extreme values of wind pressure coefficient along the circumference of the cylinder are given in Fig. 14(a) for the flat-roof tank and Fig. 14(b) for the dome-roof tank, respectively. For the flat-roof tank, the pattern of either the maximum or the minimum seems similar to the mean pressure coefficient distribution. For the dome-roof tank, only the maximum value distribution is similar to the mean coefficient pattern. The minimum value present a deviation from the mean coefficient especially on the wake region (θ=135~180°). For both models, an instantaneous pressure coefficient can present a wide range from the maximum value to minimum value. The spatial correlation analysis may help to understand the feature of the wind pressure fluctuating.
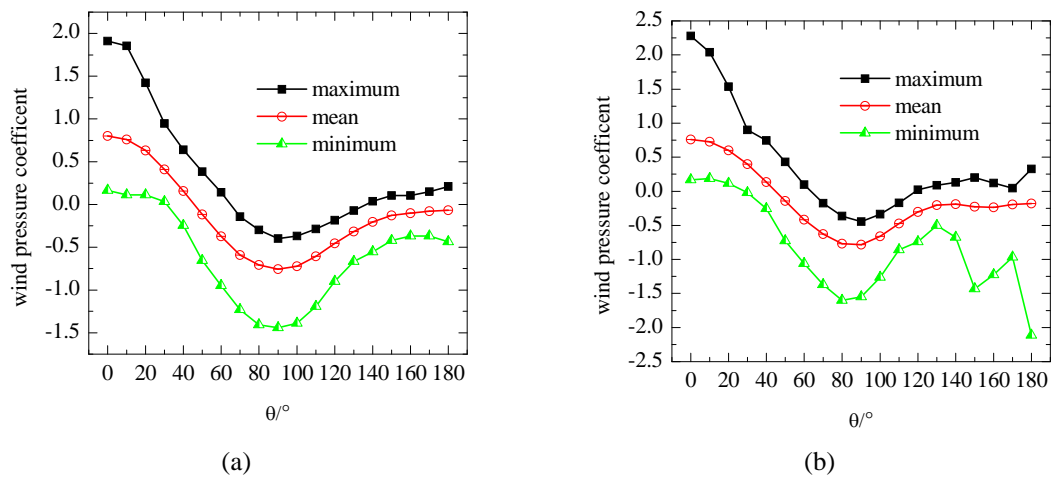

(a)   (b)

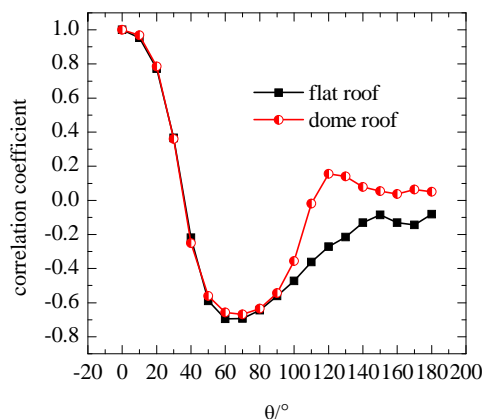Fig. 14 Envelope load (a) flat-roof tank and (b)dome-roof tank

Fig. 15 Correlation coefficient of wind pressures

The distributions of the correlation coefficients between the wind pressures at the stagnation taps and the other taps at the same height on the cylinder for both models are shown in Fig. 15. The pattern of the correlation coefficients distribution is similar to that of the mean pressure distribution in some degree. In the windward region, the correlation coefficients are positive. And in the side, the correlation coefficients are negative. In the windward region and side, the values for both models agree well with each other. But in the wake region, the values present a significant deviation though the magnitude is relatively smaller, approaching zero. It reveals that the roof have a remarkable influence on the flow on the wake region.

4.5 POD analysis

The wind pressure field on building is usually a complex and random field, the Proper Orthogonal Decomposition (POD) method is a powerful and efficient tool to investigate the essence of such a field, by resolving the fluctuating pressure into two principal components: eigen values and orthogonal eigenvector modes (Chatterjee 2000).

The first two eigenvector modes obtained from the POD analysis are shown in Fig. 16 for the flat-roof tank and in Fig. 17 for the dome-roof tank, respectively. Data have been normalized by their maximum value for all series. The first mode shapes agree well with the distribution of mean pressure in some degree for both models but the second mode shapes are no longer similar to the pattern of mean pressure.

Some previous study found that the first and second mode shapes obtained from POD analysis agree well with the distribution of the mean pressure coefficient and its first-derivative based on a two-dimensional quasi-steady as sumption (Macdonald *et al*. 1988, Uematsu 2008). However, results from present test indicate that this assumption is not always valid.
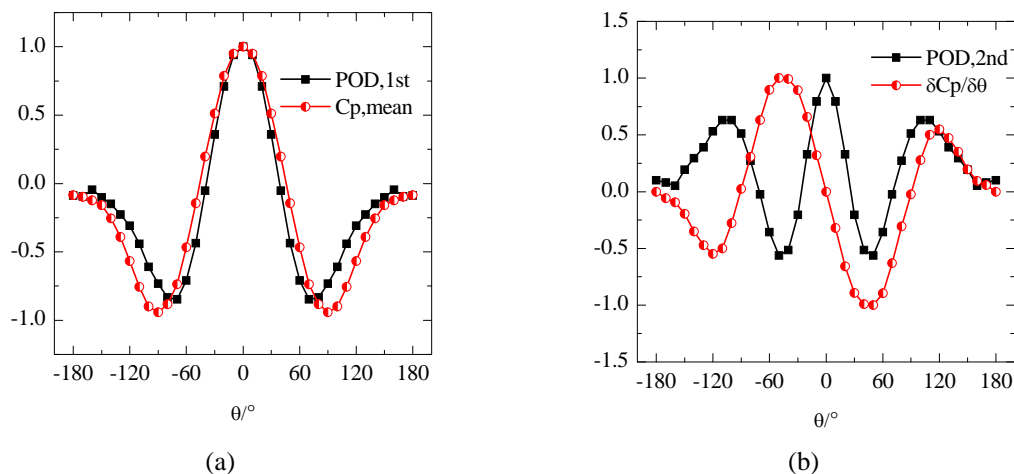

Fig. 16 Orthogonal eigenvector modes of flat-roof tank (a) first mode and (b) second mode
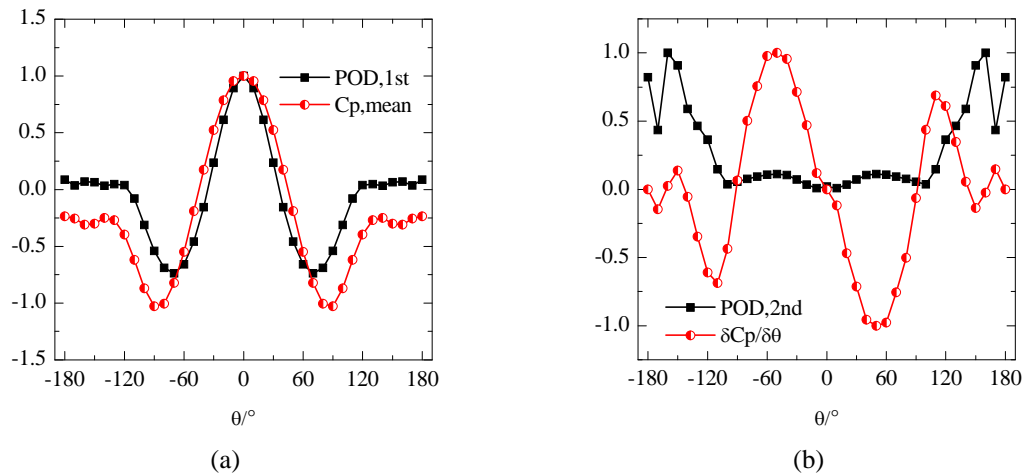
Fig. 17 Orthogonal eigenvector modes of dome-roof tank (a) first mode and (b) second mode

5. Conclusions

This paper has been concerned with the wind loads on super-large cylindrical tanks with a fixed roof. Based on above work, the main conclusions can be summarized as follows.

1. The wind loads are closely related to the behavior of flow around the structure. For either flat-roof tanks or dome-roof tanks, the mean pressures on the cylinder are positive on the windward area and negative on the sides where the flow begins to separate. The mean pressures are also negative on the wake area but the magnitudes are smaller because of the weak of vortex. It is shown that fixed roofs have no considerable influence on the mean pressure distributions of cylindrical wall in general.

2. Mean pressures on the whole roof are negative for either flat-roof tanks or dome-roof tanks, but the pressure distribution present significant difference. Suctions decrease from the windward eaves to leeward eaves for the flat roof, while for the dome roof, the suctions increase from the windward leading edge to the apex of roof and then decrease to the trailing edge. It is because that the geometric transition between the cylinder and the roof can change the behavior of the flow separation.

3. Highly non-Gaussian feature is found in either flat-roof tanks or dome-roof tanks. It is probably because of the existence of the organized vortexes when the incoming flow passes around the structure. Different series of pressures present a strong correlation.

4. The distributions of wind pressure when stationary point experiences a peak pressure are obtained by using the conditional sampling technique. It is shown that the patterns of wind pressure obtained from conditional sampling are similar to the mean pressure patterns and only slightly differences are observed for both models with different roofs. Therefore, instantaneous pressure for buckling analysis can be calculated based on the mean pressure and a guest factor.

5. For either flat-roof tanks or dome-roof tanks, an instantaneous pressure coefficient can present a wide range from the maximum value to minimum value. Therefore the spatial correlation must be included in wind pressure analysis considering the fluctuation.

6. POD analysis on the test results indicates that the quasi-steady assumption is not suitable to

predict the flow behavior in present study.

Acknowledgments

References

Chatterjee, A. (2000), "An introduction to the proper orthogonal decomposition", *Current Science*, **78**(7), 808-817

Godoy, L.A (2007), "Performance of storage tanks in oil facilities following hurricanes katrina and rita", *J. Perform. Constr. Fac.*, **21**(6), 441-449.

Godoy, L.A. and Jaca, R.C. (2010), "Wind buckling of metal tanks during their construction", *Thin Wall. Struct.*, **48**(6), 453-459.

Holroyd, R.J. (1983), "On the behaviour of open-topped oil storage tanks in high winds. Part I. Aerodynamic aspects", *J. Wind Eng. Ind. Aerod.*, **12**(3), 329-352.

Koo, C., Uematsu, Y., Kondo, K. and Okubo, K. (2010), "Wind Loads for designing open-topped oil storage tanks", *Proceedings of the International Association for Shell and Spatial Structures (IASS) Symposium*: *Spatial Structures – Permanent and Temporary*, Shanghai, China, November.

MacDonald, P.A., Kwok, K.C.S. and Holmes, J.D. (1988), "Wind loads on circular storage bins, silos and tanks: I. Point pressure measurements on isolated structures", *J. Wind Eng. Ind. Aerod.*, **31**, 165-187.

Maher, F.J. (1966), "Wind loads on dome-cylinders and dome-cone shapes", *J. Struct. Div. - ASCE*, **91**(3), 79-96.

Myers, P. (1997), *Aboveground storage tanks*, McGraw-Hill, New York, American.

Portela, G. and Godoy, L.A. (2005a), "Wind pressures and buckling of cylindrical steel tanks with a dome roof", *J. Constr. Steel Res.*, **61**(6), 786-807.

Portela, G. and Godoy, L.A. (2005b), "Wind pressures and buckling of cylindrical steel tanks with a conical roof", *J. Constr. Steel Res.*, **61**(6), 808-824.

Purdy, D.M, Maher, P.E, Frederick, D. (1967), "Model studies of wind loads on flat-top cylinders", *J. Struct. Div. - ASCE*, **93**, 379-395.

Rotter, J.M. (2009), "Silos and tanks in research and practice: state of the art and current challenges", *Proceedings of Symposium on Evolution and Trends in Design, Analysis and Construction of Shell and Spatial Structures, IASS*. Valencia, Spain, September.

Sosa, E.M. (2005), *Computational buckling analysis of cylindrical thin-walled aboveground tanks*, Ph.D. Dissertation, University Of Puerto Rico, Mayagüez Campus, Mayagüez.

National Standard of P. R. China (2012), *Load code for the design of building structures*, Beijing, China.

Sabransky, I.J. and Melbourne, W.H. (1987), "Design pressure distribution on circular silos with conical roofs", *J. Wind Eng. Ind. Aerod.*, **26**(1), 65-84.

Sun, Y., Wu, Y. and Lin, Z. *et al.* (2007), "Non-Gaussian features of fluctuating wind pressures on long span roofs", *China Civil Eng. J.*, **40**(4), 1-5. (In Chinese)

Uematsu, Y., Koo, C. and Kondo, K. (2008), "Wind loads on open-topped oil-storage tanks", *Proceedings of the 6th International Colloquium on Bluff Body Aerodynamics and Application*, Milan, Italy, July.

CC